A generalized Drude model for doped silicon at terahertz frequencies derived from microscopic transport simulation

K. J. Willis, S. C. Hagness, and I. Knezevic

Articles you may be interested in

Anisotropic propagation and upper frequency limitation of terahertz waves in graphene
Appl. Phys. Lett. **103**, 071904 (2013); 10.1063/1.4818683

Multiphysics simulation of high-frequency carrier dynamics in conductive materials
J. Appl. Phys. **110**, 063714 (2011); 10.1063/1.3627145

Defect modification and energy extraction in a one-dimensional terahertz photonic crystal
J. Appl. Phys. **109**, 024902 (2011); 10.1063/1.3537824

Silicon based microfluidic cell for terahertz frequencies
J. Appl. Phys. **108**, 013102 (2010); 10.1063/1.3456175

Terahertz conductivity of doped silicon calculated using the ensemble Monte Carlo/finite-difference time-domain simulation technique
Appl. Phys. Lett. **96**, 062106 (2010); 10.1063/1.3308491

A generalized Drude model for doped silicon at terahertz frequencies derived from microscopic transport simulation

K. J. Willis,[a)] S. C. Hagness,[b)] and I. Knezevic[c)]

Department of Electrical and Computer Engineering, University of Wisconsin–Madison,
1415 Engineering Dr., Madison, Wisconsin 53706-1691, USA

Unveiling the full potential of doped silicon for electronic, photonic, and plasmonic application at THz frequencies requires a thorough understanding of its high-frequency transport properties. In this letter, we present a comprehensive numerical characterization of the frequency-dependent (0–2.5 THz) complex conductivity of silicon at room temperature over a wide range of doping densities ($10^{14} - 10^{18}$ cm^{-3}). The conductivity was calculated using a multiphysics computational technique that self-consistently couples ensemble Monte Carlo (EMC) simulation of carrier transport, the finite-difference time-domain (FDTD) solution to Maxwell's equations, and molecular dynamics (MD) for the treatment of short-range Coulomb interactions. Our EMC/FDTD/MD numerical results complement the experimental data that only exist for a select few doping densities. Moreover, we show that the computed complex conductivity of Si at THz frequencies can be accurately described by a generalized Drude (GD) model with doping-dependent parameters that capture the cross-over from phonon-dominated to Coulomb-dominated electron transport as the doping density increases. The simplicity of the GD model enables one to readily compute the complex conductivity of silicon for any doping density within the range studied here. © 2013 American Institute of Physics. [http://dx.doi.org/10.1063/1.4798658]

Silicon is at the focus of considerable efforts to combine electronic and optical systems on a single chip.[1,2] Recent advances in silicon photonics include nanolasers,[3] plasmonic waveguides,[4] and electro-optic modulators.[5,6] Silicon nano-membranes have been developed into flexible microwave transistors[7] and flexible photonic-crystal Fano filters,[8] while silicon-based plasmonic devices promise advances in the efficiency of high-performance computing systems.[1]

Pure undoped silicon is an attractive material for THz-frequency optics[9] because it is almost completely transparent and nondispersive under THz-frequency radiation. The THz frequency range, with frequencies 0.1–10 THz and wavelengths 30–3000 μm, lies between the microwave and optical frequency ranges and offers opportunities for high resolution tomographic imaging,[10,11] genetic diagnostics,[12] cellular imaging,[13,14] nondestructive testing,[15–17] and nonlinear THz spectroscopy at ultrashort timescales.[18] However, silicon becomes opaque to THz radiation even at low levels of doping[19] owing to the interaction of free carriers with the fields.[9] The THz transport properties of Si have been characterized experimentally only for a few select doping densities,[19,20] and their frequency dependence is not adequately described by the Drude model.[21,22] Unlocking the full potential of doped silicon for a myriad of THz electronic, photonic, and plasmonic application requires a better understanding of its high-frequency transport properties.

In this letter, we present a comprehensive numerical characterization of THz transport in silicon. We compute the room-temperature conductivity of silicon over a broad range of frequencies (0–2.5 THz) and doping densities ($n_0 = 10^{14} - 10^{18}$ cm^{-3}). These frequencies are comparable to the characteristic carrier scattering rates, so the common quasistatic approaches are difficult to justify.[23,24] Instead, it becomes necessary to fully describe the dynamics of both charge carriers and electromagnetic waves, as well as their mutual interaction. To that end, we employ a recently developed multiphysics computational technique[25,26] that accurately describes carrier dynamics under high-frequency electromagnetic excitation. The technique self-consistently couples ensemble Monte Carlo (EMC) stochastic simulation of carrier transport in silicon with the finite-difference time-domain (FDTD) solution to Maxwell's equations and a molecular dynamics (MD) implementation of the short-range Coulomb interactions (electron-electron and electron-ion) and the exchange interaction among electrons. The conductivity computed by the combined EMC/FDTD/MD technique shows excellent agreement with experimental data for the few doping densities for which experimental results are available in the literature.[20,26] We show that the complex conductivity data can be fitted well by a generalized Drude (GD) analytical model with doping-dependent fitting parameters. The GD model is flexible enough to capture the cross-over from phonon-dominated to Coulomb-dominated transport as the doping density increases. The simple GD analytical fit, with appropriate doping-dependent parameters, can be readily used to predict the complex conductivity of arbitrarily doped samples within the investigated range.

As the doping density of bulk silicon samples increases, the relative importance of electron-phonon interaction for electronic transport diminishes in favor of the Coulomb interaction, whose long-range and short-range components are

---

[a)]Current address: AWR Corp., Mequon, Wisconsin 53092, USA. Email: keelywillis@gmail.com.
[b)]Email: hagness@engr.wisc.edu.
[c)]Email: knezevic@engr.wisc.edu.

102, 122113-1

treated via FDTD and MD, respectively, in the three-pronged EMC/FDTD/MD simulation. At room temperature and low doping densities ($n_0 < 10^{16}$ cm^{-3}), electron dynamics in silicon is dominated by electron-phonon interaction, i.e., by intravalley scattering via acoustic phonons and intervalley scattering via long-wavevector optical and acoustic phonons.[27,28] At n_0 above 10^{16} cm^{-3}, both Coulomb interactions and carrier-phonon scattering influence ensemble relaxation, and carrier mobility falls rapidly.

For high doping densities, at or above 10^{18} cm^{-3}, the short-range Coulomb interactions among carriers and between carriers and ions strongly affect transport. The force acting on an electron within a few Angstroms of an ion deviates from the representation of point-charge interaction according to Coulomb's law.[29–31] Rather than describing such interactions with the bare Coulomb force, it is appropriate to consider the dopant ion charge as distributed with a Gaussian profile of characteristic half-width r_d.[26] At these high doping densities, the exchange interaction among electrons, stemming from the Pauli exclusion principle, can also significantly affect materials properties.[32–35] The exchange interaction manifests itself as a reduction in the force among same-spin electrons.[32–35] By using minimum-uncertainty Gaussian wave packets of radius r_c to describe electrons,[32–35] the electron charge is distributed over a finite volume for all direct-force calculations among carriers, and the force is reduced for same-spin electrons.[26]

We determine the appropriate electron radius, r_c, and ion radius, r_d, to be used in the EMC/FDTD/MD solver in the following manner. For each n_0 of interest, we calculate the *dc* conductivity, $\sigma(0)$, for a wide range of r_c and r_d values.[26] The optimal r_c and r_d are chosen as the values for which $\sigma(0)$ accurately reproduces the known[36] *dc* conductivity of the material, σ_0. *dc* conductivity is fairly insensitive to r_c, so we choose the value corresponding to the effective radius of the Hartree-Fock exchange-correlation hole[26,37]

$$r_c = \exp\left(-\frac{\ln n_0}{3} + 17.366\right), \quad (1)$$

where n_0 is given in cm^{-3}. At low doping densities, conductivity does not vary appreciably with r_d either, but there is a lower limit on r_d, found to be about 1.1 Å, to ensure that electrons passing too close to an ion do not accelerate to unphysical speeds or deflect at unphysical angles.[26] With increasing doping density, electron-ion interactions become increasingly important in electron transport, and conductivity becomes considerably more sensitive to the choice of r_d. For doping densities above 10^{15} cm^{-3}, the optimal r_d values are of order 2–4 Å, the same order of magnitude as the radii used for the Lennard-Jones potential in the molecular dynamics simulation of phosphorus compounds.[38] Table I shows the optimal values of r_c and r_d for phosphorus-doped silicon for each value of n_0.

TABLE I. Calculated r_c and r_d values from $\sigma(0)$.

n_0 [cm^{-3}]	10^{14}	10^{15}	10^{16}	10^{17}	10^{18}
r_c [Å]	750	350	160	75	35
r_d [Å]	1.1	1.1	2	3	3.5

We use the EMC/FDTD/MD technique to compute the frequency-dependent complex conductivity, $\sigma(\omega)$, of *n*-type, phosphorous-doped silicon at room temperature for electromagnetic wave excitations of frequencies 0–2.5 THz. In the simulation, an electromagnetic wave is launched into the silicon sample, and the conductivity inside the sample is computed from the local grid-based electric fields and currents.[26] The real part of $\sigma(\omega)$ corresponds to power dissipation in the material, while the imaginary part of $\sigma(\omega)$ describes the phase shift between the electric field and current density in the material. In choosing the grid cell size and time step, we must strike a balance between the FDTD simulation requirements (grid cell size below 1/10 of the relevant wavelength and a time step obeying the Courant criterion[39]) with the requirements stemming from other parts of the combined code. For instance, to control the MD computational burden, a grid cell should on average not accommodate more than two or three electrons, which puts an upper bound on the grid cell size, making it very small for higher doping densities and prolonging the simulation. On the other hand, a grid cell too small to fit a whole electron or dopant inside it can result in instabilities related to artificial electron localization. A detailed account of these numerical considerations can be found in the appendix of Ref. 26.

Fig. 1 shows the real and imaginary parts of the complex conductivity for doping densities $10^{14} - 10^{18}$ cm^{-3}, calculated by EMC/FDTD/MD (circles) along with an analytical GD model fit (solid curves) to the simulation results and the Drude model prediction (dashed curves). The GD model conductivity, $\sigma_{GD}(\omega)$, is given by

$$\sigma_{GD}(\omega) = \frac{\sigma(0)}{[1 - (i\omega\tau_{GD})^{1-\alpha}]^\beta}. \quad (2)$$

Here, α and β are real numbers, where $0 \le \alpha, \beta \le 1$. For $\alpha = 0$ and $\beta = 1$, GD reduces to the Drude model, which assumes that carrier relaxation time τ is independent of energy so a single value, $\tau_{\sigma(0)}$, describes the time response of the entire ensemble. This assumption is not realistic for semiconductors, where electrons scatter with phonons, charged impurities, and other carriers, and the total relaxation time has a pronounced energy dependence.[28] With $\alpha \ne 0$ and $\beta \ne 1$, the GD model allows for a continuum of relevant relaxation times, such that the distribution of the logarithms of relaxation times, $\ln(\tau)$, is peaked around the logarithm of the most prominent time, $\ln(\tau_{GD})$.[40–42] α governs the width while β determines the symmetry of the $\ln(\tau)$ distribution.[43] In the Cole-Cole (CC) model, given by Eq. (2) with $\beta = 1$ and $0 \le \alpha < 1$, the distribution of $\ln(\tau)$ is symmetric with respect to $\ln(\tau_{GD})$, with a width that increases with increasing α.[43] The Cole-Davidson (CD) model, given by Eq. (2) with $\alpha = 0$ and $0 \le \beta \le 1$, describes an asymmetric $\ln(\tau)$ distribution, which is zero for $\tau > \tau_{GD}$ and decays with decreasing τ for $\tau < \tau_{GD}$.[43] Here, we also vary τ_{GD} in order to capture the situation in which the peak position of the relaxation-time distribution does not coincide with the $\tau_{\sigma(0)}$ from the *dc* Drude-model conductivity.[44]

Table II shows the known (measured) *dc* conductivity of *n*-type silicon for each value of n_0, the calculated *dc* conductivity from EMC/FDTD/MD and the corresponding relaxation
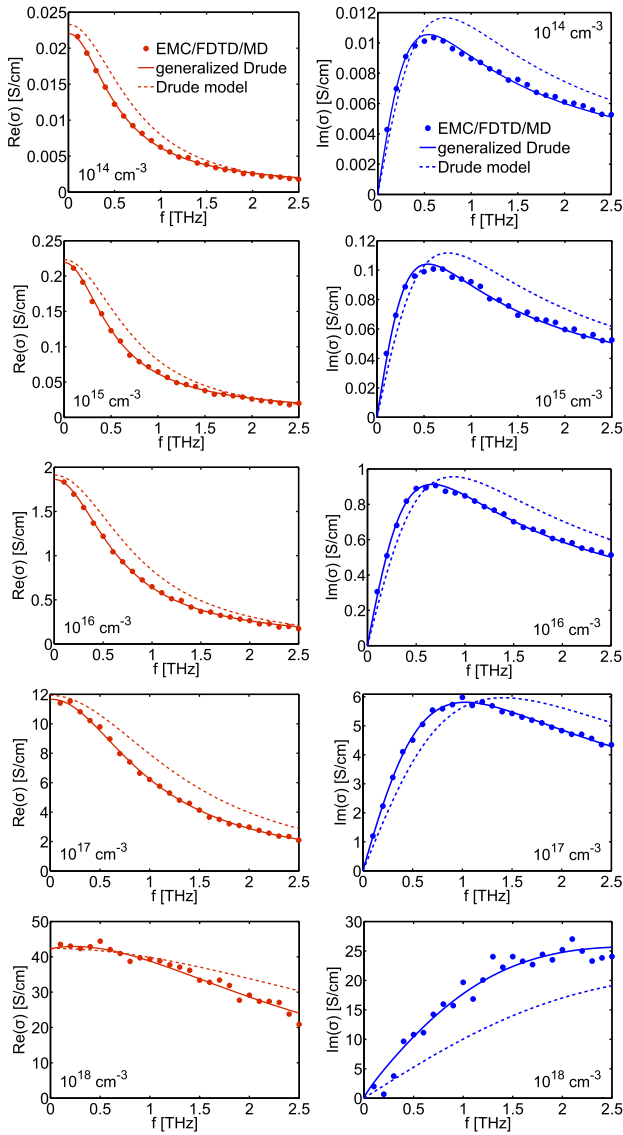
FIG. 1. Real part (left) and imaginary part (right) of the room-temperature complex conductivity of n-type, phosphorous-doped silicon at THz frequencies, for doping densities of $10^{14} - 10^{18}$ cm^{-3}. Solid circles are the data obtained from EMC/FDTD/MD simulations, with the appropriate r_c and r_d listed in Table I. The dashed curves correspond to the Drude model, while the solid curves correspond to the GD fit [Eq. (2)], with the appropriate values of parameters α, β, and τ_{GD} given in Table II.

TABLE II. Measured dc conductivity σ_0,[36] calculated dc conductivity $\sigma(0)$ based on EMC/FDTD/MD simulation and the corresponding scattering time $\tau_{\sigma(0)}$ extracted based on the Drude model, as well as the generalized Drude model fitting parameters (τ_{GD}, α, and β) presented for different doping densities n_0.

n_0 [cm^{-3}]	10^{14}	10^{15}	10^{16}	10^{17}	10^{18}
σ_0 [S/cm]	0.023	0.223	1.912	11.93	42.37
$\sigma(0)$ [S/cm]	0.022	0.219	1.864	11.65	42.17
$\tau_{\sigma(0)}$ [ps]	0.209	0.207	0.181	0.110	0.040
τ_{GD} [ps]	0.341	0.336	0.264	0.168	0.071
α	0.03	0.02	0.02	0.04	0.19
β	0.84	0.84	0.88	0.89	0.82

parameters than any of the others, this is not surprising. We gain insight into the appropriate regimes for the different models by considering the quality of the fit of each model to the conductivity data provided by EMC/FDTD/MD. For $n_0 = 10^{14} - 10^{16}$ cm^{-3}, CD fits nearly as well as GD, and much better than either CC or Drude. For $n_0 = 10^{17}$ cm^{-3}, none among the CD, CC, or Drude models fits particularly well, while GD still fits very well. For the highest n_0 in our tests, 10^{18} cm^{-3}, CC fits nearly as well as GD, and CD and Drude fit equivalently poorly. These trends indicate that we may assume an almost completely asymmetric $\ln(\tau)$ distribution, with $\alpha = 0$, in the low-n_0 regime where carrier relaxation is dominated by electron-phonon interactions. In the high-n_0 range, in which the short-range Coulomb interactions dominate carrier relaxation, we may assume an almost completely symmetric distribution of relaxation times, with $\beta = 1$. At the midrange n_0-value of about 10^{17} cm^{-3}, where an interplay between Coulomb and electron–lattice interactions dominates transport, a relaxation time distribution that has both symmetric and asymmetric components is needed to accurately capture the data.

In conclusion, we have presented a calculation of the complex conductivity of silicon at room temperature, under electromagnetic wave excitation with frequencies from 0 to 2.5 THz and for a wide range of doping densities ($10^{14} - 10^{18}$ cm^{-3}). Our EMC/FDTD/MD numerical results represent the first comprehensive characterization of the THz-frequency conductivity of silicon over a wide range of doping densities, thereby complementing the experimental data that only exist for select doping densities. Moreover, we have shown that the conductivity data can be accurately fitted based on a GD model [Eq. (2)], with doping-dependent fitting parameters (Table II). The GD model's flexibility is necessary to accurately capture the EMC/FDTD/MD simulation data over the wide range of doping densities, in which a cross-over from phonon-dominated to Coulomb-dominated

time according to the Drude model for each n_0. The generalized Drude model fitting parameters (τ_{GD}, α, and β) are also shown. We see that $\tau_{GD} > \tau_{\sigma(0)}$ for every n_0: the peak relaxation time calculated from EMC/FDTD/MD data is consistently longer than the characteristic relaxation time predicted by the Drude model. In addition, for $n_0 \leq 10^{17}$ cm^{-3}, $\alpha \approx 0$ and β is roughly constant. In this case, the GD conductivity reduces to the CD model. For $n_0 = 10^{18}$ cm^{-3}, α and β both change from the values they held at lower doping densities, so the material is no longer accurately described by the CD model.

Table III summarizes the quality of the fit based on the GD, CC, CD, and Drude models to the EMC/FDTD/MD data; the quality of the fit is represented by the maximal relative deviation (in percent) of the data from the fit over the entire frequency range. The GD model gives the best fit for every value of n_0; since the GD model has more free

TABLE III. Relative error (in percent) for the generalized Drude, Cole-Davidson, Cole-Cole, and Drude model fits.

n_0 [cm^{-3}]	10^{14}	10^{15}	10^{16}	10^{17}	10^{18}
ε_{GD}	0.814	0.986	0.645	0.820	3.381
ε_{CD}	0.999	1.093	0.940	1.201	7.635
ε_{CC}	2.448	2.670	1.665	1.398	3.469
ε_{D}	2.448	2.670	1.665	1.398	7.635

transport occurs. The simplicity of the GD model enables one to readily compute the complex conductivity of silicon for any doping density within the range we studied here, based on interpolating the fitting parameters.

[1]V. R. Almeida, C. A. Barrios, R. R. Panepucci, and M. Lipson, Nature (London) **431**, 1081 (2004).

[2]J. A. Dionne, K. Diest, L. A. Sweatlock, and H. A. Atwater, Nano Lett. **9**, 897 (2009).

[3]M. T. Hill, Nat. Photonics **5**, 130 (2011).

[4]I. D. Rukhlenko, M. Premaratne, and G. P. Agrawal, Opt. Express **19**, 206 (2011).

[5]J. H. Liu, C. L. Chen, H. T. Lue, and J. T. Lue, Meas. Sci. Technol. **13**, 2032 (2002).

[6]Q. Xu, B. Schmidt, S. Pradhan, and M. Lipson, Nature (London) **435**, 325 (2005).

[7]H.-C. Yuan and Z. Ma, Appl. Phys. Lett. **89**, 212105 (2006).

[8]W. Zhou, Z. Ma, H. Yang, Z. Qiang, G. Qin, H. Pang, L. Chen, W. Yang, S. Chuwongin, and D. Zhao, J. Phys. D: Appl. Phys. **42**, 234007 (2009).

[9]D. Grischkowsky, S. Keiding, M. van Exter, and C. Fattinger, J. Opt. Soc. Am. B Opt. Phys. **7**, 2006 (1990).

[10]B. Ferguson and X. Zhang, Nature Mater. **1**, 26 (2002).

[11]D. M. Mittleman, S. Hunsche, L. Boivin, and M. C. Nuss, Opt. Lett. **22**, 904 (1997).

[12]M. Nagel, P. H. Bolivar, M. Brucherseifer, and H. Kurz, Appl. Phys. Lett. **80**, 154 (2002).

[13]R. M. Woodward, V. P. Wallace, R. J. Pye, B. E. Cole, D. D. Arnone, E. H. Linfield, and M. Pepper, J. Investig. Dermatol. **120**, 72 (2003).

[14]J. Nishizawa, T. Sasaki, and T. Tanno, J. Phys. Chem. Solids **69**, 693 (2008).

[15]A. Dobroiu, M. Yamashita, Y. N. Ohshima, Y. Moritam, C. Otani, and K. Kawase, Appl. Opt. **43**, 5637 (2004).

[16]D. van der Weide, Opt. Photonics News **14**, 48 (2003).

[17]P. H. Siegel, IEEE Trans. Microwave Theory Tech. **50**, 910 (2002).

[18]M. C. Hoffmann and J. A. Fülöp, J. Phys. D: Appl. Phys. **44**, 083001 (2011).

[19]M. van Exter and D. Grischkowsky, Phys. Rev. B **41**, 12140 (1990).

[20]T. I. Jeon and D. Grischkowsky, Phys. Rev. Lett. **78**, 1106 (1997).

[21]K. J. Willis, J. Ayubi-Moak, S. C. Hagness, and I. Knezevic, J. Comput. Electron. **8**, 153 (2009).

[22]J. Lloyd-Hughes and T.-I. Jeon, J. Infrared, Millim. Terahertz Waves **33**, 871 (2012).

[23]M. A. Alsunaidi, S. M. Imtiaz, and S. El-Ghazaly, IEEE Trans. Microwave Theory Tech. **44**, 799 (1996).

[24]R. O. Grondin, S. El-Ghazaly, and S. M. Goodnick, IEEE Trans. Microwave Theory Tech. **47**, 817 (1999).

[25]K. J. Willis, S. C. Hagness, and I. Knezevic, Appl. Phys. Lett. **96**, 062106 (2010).

[26]K. J. Willis, S. C. Hagness, and I. Knezevic, J. Appl. Phys. **110**, 063714 (2011).

[27]C. Jacoboni and L. Reggiani, Rev. Mod. Phys. **55**, 645 (1983).

[28]M. Lundstrom, *Fundamentals of Carrier Transport*, 2nd ed. (Cambridge University Press, 2000).

[29]B. K. Ridley, *Quantum Processes in Semiconductors*, 4th ed. (Oxford Science Publications, 1999).

[30]H. I. Ralph, G. Simpson, and R. J. Elliott, Phys. Rev. B **11**, 2948 (1975).

[31]D. Chattopadhyay and H. J. Queisser, Rev. Mod. Phys. **53**, 745 (1981).

[32]D. K. Ferry, A. M. Kriman, and M. J. Kann, Comput. Phys. Commun. **67**, 119 (1991).

[33]A. M. Kriman, M. J. Kann, D. K. Ferry, and R. Joshi, Phys. Rev. Lett. **65**, 1619 (1990).

[34]A. M. Kriman, R. P. Joshi, M. J. Kann, and D. K. Ferry, Semicond. Sci. Technol. **7**, B243 (1992).

[35]R. P. Joshi, A. M. Kriman, M. J. Kann, and D. K. Ferry, Appl. Phys. Lett. **58**, 2369 (1991).

[36]R. Hull, *Properties of Crystalline Silicon* (IET, 1999).

[37]P. Gori-Giorgi, F. Sacchetti, and G. B. Bachelet, Phys. Rev. B **61**, 7353 (2000).

[38]J.-J. Liang, R. Cygan, and T. Alam, J. Non-Cryst. Solids **263–264**, 167 (2000).

[39]A. Taflove and S. C. Hagness, *Computational Electrodynamics: The Finite-Difference Time-Domain Method, 3rd ed.* (Artech House, 2005).

[40]K. W. Wagner, Ann. Phys. **40**, 817 (1913); [Ann. Phys. **345**, 817 (2006) (in German)].

[41]W. A. Yager, J. Appl. Phys. **7**, 434 (1936).

[42]R. M. Hill and L. A. Dissado, J. Phys. C **18**, 3829 (1985).

[43]M. C. Beard, G. M. Turner, and C. A. Schmuttanmaer, Phys. Rev. B **62**, 15764 (2000).

[44]$\tau_{\sigma(0)} = \sigma(0)m^*/n_0q^2$, where $m^* = 0.26\,m_0$ is the conductivity effective mass of electrons in silicon, m_0 is the free-electron mass, and q is the elementary charge.